Characterization and dielectric properties of polyaniline–TiO_2 nanocomposites

INSTITUTE OF PHYSICS PUBLISHING NANOTECHNOLOGY
Nanotechnology **15** (2004) 1277–1283 PII: S0957-4484(04)80772-4

Characterization and dielectric properties of polyaniline–TiO_2 nanocomposites

Ashis Dey[1], **Sukanta De**[1], **Amitabha De**[2] **and S K De**[1]

[1] Department of Materials Science, Indian Association for the Cultivation of Science, Jadavpur, Kolkata-700 032, India
[2] Chemical Sciences Division, Saha Institute of Nuclear Physics, 1/AF Bidhannagar, Kolkata-700 064, India

Received 4 May 2004
Published 23 July 2004
Online at stacks.iop.org/Nano/15/1277
doi:10.1088/0957-4484/15/9/028

Abstract
Nanocomposites of polyaniline (PANI)–titanium dioxide (PANI–TiO_2) are prepared from a colloidal sol of TiO_2 nanoparticles. The dc and ac conductivities of samples with different concentrations of PANI have been investigated as a function of frequency and temperature. The dc conductivity follows three-dimensional variable range hopping. The ac conductivity has been interpreted as a power law of frequency. The temperature variation of the frequency exponent suggests a correlated barrier hopping conduction process in the nanocomposites. A very large dielectric constant of about 3700 at room temperature has been observed. An electric modulus presentation is used to interpret the dielectric spectra. The interface between polyaniline and TiO_2 plays an important role in yielding a large dielectric constant in the nanocomposite.

1. Introduction

Polyaniline is the most attractive conducting polymer because of its low cost, high environmental stability, good electrical conductivity and potential applications in molecular electronics [1]. The electrical properties of polymers can be modified by addition of inorganic fillers. Nanoscale particles are more attractive due to intriguing properties arising from the nanosize and large surface area. The insertion of nanoscale fillers may improve the electrical and dielectric properties of the host polymers. Titanium dioxide (TiO_2) is a very promising material for a large number of applications in different fields in catalysis, dielectric ceramics, solar cells and optoelectronic devices [2, 3]. Among various polymorphs, the anatase phase of TiO_2 is a wide bandgap (3.2 eV) semiconductor.

Polymer–semiconductor nanocomposites generate a new field for the development of advanced materials in science and technology [4]. The properties of nanocomposites are quite different from the constituent materials due to interfacial interactions between nanostructured semiconductors and polymers. The properties of these materials can easily be tuned to the desired application through the variation of particle size, shape and distribution of the nanoparticles. The main difficulty is the synthesis of inorganic nanoparticles in the matrix of conducting polymers which are infusible and are not soluble in common solvents. The aggregation of nanoparticles with high surface energy also limits the preparation of nanostructured composites. A homogeneous nanocomposite of desired properties can be prepared by incorporating nanocrystalline TiO_2 particles from the colloidal suspension.

The composites of TiO_2 with different polymers such as conducting polyaniline (PANI) [5–8], poly(phenylenevinylene) (PPV) [9] and poly(methylmethacrylate) (PMMA) [10] have been studied in the last few years. Most of the studies are concentrated on optical properties of the polymer surface modified TiO_2 nanoparticles. The materials with high dielectric constant are very useful in integrated electronic circuits such as capacitor and gate oxides. The primary criteria of such materials is to improve the leakage current and break-down voltage. Submicron thickness gate materials are required to fabricate small scale metal oxide devices. Synthesis of materials with large dielectric constant is very important for development of new generation dynamic random access memories and micro-electromechanical systems. High dielectric constants are essential to fulfil these properties. The large bandgap and high dielectric constant of TiO_2 and the good thermal stability of polyaniline indicates that the PANI–TiO_2 nanocomposite may yield high dielectric constant. Transport

Table 1. Weight percentage of aniline (x), room temperature dc conductivity (σ_{RT}), σ_0, T_0 and room temperature dielectric constant (ϵ_1) at the lowest measurable frequency.

Sample	x	σ_{RT} (10^{-4}) (S cm^{-1})	σ_0 (S cm^{-1})	T_0 (10^6) (K)	ϵ_1
S1	88.4	2.38	63.43	6.52	3700
S2	92.7	3.17	3.12	2.01	3327
S3	96.2	5.55	2.04	1.43	1755
S4	100.0	6.85	0.07	1.38	394

and dielectric properties of conducting polymers containing nanosized semiconductors have not yet been studied in detail. In this work we present the transport and dielectric properties of PANI–TiO_2 nanocomposites at low temperature and high frequency.

2. Experimental details

Aniline and ammonium peroxydisulfate (APS) are purchased from E Merck (India). Aniline is distilled twice under reduced pressure and stored below 4 °C in nitrogen atmosphere. APS is used as received.

Titanium dioxide TiO_2 colloid is synthesized at room temperature by the acid hydrolysis of titanium isopropoxide. In a typical synthesis 8 g of titanium isopropoxide is dissolved in 50 ml of 0.1(N) HCl to get a clear solution. This solution is added dropwise to 500 ml of double distilled water under constant stirring. pH of the resulting solution is adjusted using dilute NH_4OH until it becomes 3. Thus the white coloured colloid formed is dialysed until free from ions and stored in a 500 ml volumetric flask. This colloid sol is used to prepare the nanocomposites.

The polyaniline (PANI)–TiO_2 nanocomposite is prepared as follows. Different volumes of aniline (0.3–1 ml) are injected into 25 ml of TiO_2 colloid under ultrasonic action to reduce the agglomeration of TiO_2 nanoparticles. 1.5 M of an acidic aqueous solution of APS (precooled) using varying amounts of concentrated HCl and keeping a 1:1.25 monomer:APS mole ratio is then added dropwise under sonication. The polymerization is allowed to proceed for 24 h maintaining the temperature at 0–5 °C. The composite comes out as a bright green residue. The solution is then washed several times with 1.5 M HCl and deionized water under ultra-centrifugation followed by drying in a vacuum oven at 60 °C for 24 h to obtain a fine green powder. Three different compositions with varying concentration of aniline and pure PANI as shown in table 1 are investigated in detail.

3. Characterization

Particle content of the colloidal TiO_2 sol is measured by freeze drying 25 ml of the sol followed by solvent evaporation at −35 °C using a lyophilizer. The dried particles are weighed until a constant weight is achieved. Particle size of the bare colloid and the nanocomposites and the nature of interaction between the conducting and insulating components are determined from transmission electron microscopic studies (Hitachi 600). Infrared (IR) spectra of the bare polymer and the nanocomposite samples pelletized with KBr are taken with a Fourier-transform infrared (FTIR) spectrometer (Perkin-Elmer model 1600). X-ray diffraction patterns of the nanocomposites are taken using a Philips diffractometer (PW 1710) using Cu Kα radiation.

The temperature dependent dc conductivity is measured by the standard four-probe method. The complex dielectric constants are obtained from the measurements of capacitance (C) and dissipation factor (D) by a 4192A Agilent impedance analyser up to the frequency of 2.5 MHz at different temperatures. The real part of dielectric constant ϵ_1 is evaluated by the relation $C = \epsilon_1 A/t$, A is the area and t is the thickness of the sample. The imaginary component is calculated from the dissipation factor, $\epsilon_2 = D\epsilon_1$. The electrical contacts are made by silver paint.

4. Results and discussion

The transmission electron micrograph (TEM) of the bare colloid and the nanocomposite (S1) are shown in figures 1(a) and (b) respectively. The colloid particles are polydispersed and are of spherical shape with uniform diameter lying in the range from 10 to 25 nm. After the formation of the composites the particles (dark shaded) are found to be entrapped into polyaniline (light shaded) chains. The immediate conclusion is that the colloid particles are not simply mixed up or blended with the polymer; they are rather encapsulated by the polyaniline chains. This fact is also supported by XRD and FTIR analysis. Figure 2 shows the FTIR spectra of polyaniline (PANI) doped with HCl and PANI–TiO_2 nanocomposite samples S1, S2 and S3 respectively. The characteristic peaks of HCl doped PANI are assigned as follows. The band at 1560 and 1474 cm^{-1} are attributed to the C=N and C=C stretching modes of vibration for the quinonoid and benzenoid units, while the bands at 1303 and 1242 cm^{-1} are assigned to the C–N stretching mode of benzenoid units. The band at 1108 cm^{-1} is due to quinonoid unit of doped PANI. The peak at 795 cm^{-1} is attributed to C–C and C–H for the benzenoid unit. The incorporation of TiO_2 in the nanocomposites leads to small shift of some FTIR peaks in PANI.

Figure 3 shows the the characteristic peaks of x-ray diffraction (XRD) of sample S1. The spectra reveal the presence of the anatase phase of titania in the nanocomposites. The crystallite size of the TiO_2 nanoparticles in composite sample S1 is calculated following Scherrer's relation (using the 101 face) [11]

$$D = K\lambda/\beta\cos\theta \tag{1}$$

where $K = 0.89$, D represents the crystallite size (nm), λ the wavelength of Cu Kα radiation and β the corrected value at half width of the diffraction peak. At $2\theta = 25.36°$, (101), which is the characteristic peak of TiO_2, is chosen to calculate the average diameter and it comes out to be 8 nm, which is consistent with that obtained from TEM studies.

The dc conductivity $\sigma(RT)$ at room temperature for various compositions are shown in table 1. The weight percentage of conducting PANI is much higher than 13% of the classical percolation threshold. As a result of this the conductivity does not change significantly with the increase of conducting PANI fraction. The temperature dependence of conductivity for three different compositions and pure doped

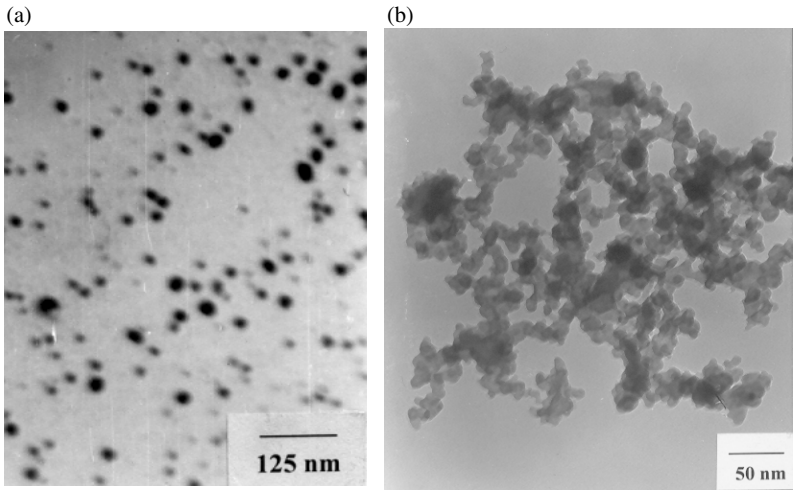

Figure 1. Transmission electron micrograph of (a) TiO_2 colloid and (b) PANI–TiO_2 nanocomposite sample S1.

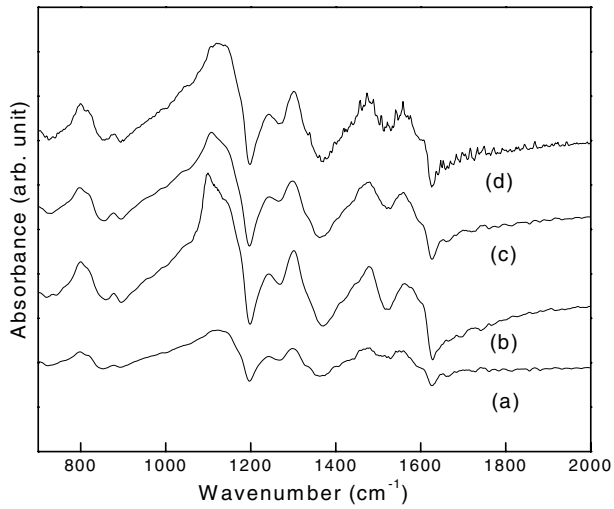

Figure 2. Fourier-transform infrared (FTIR) spectra of (a) HCl doped PANI(S4), (b) nanocomposite S1, (c) nanocomposite S2 and (d) nanocomposite S3.

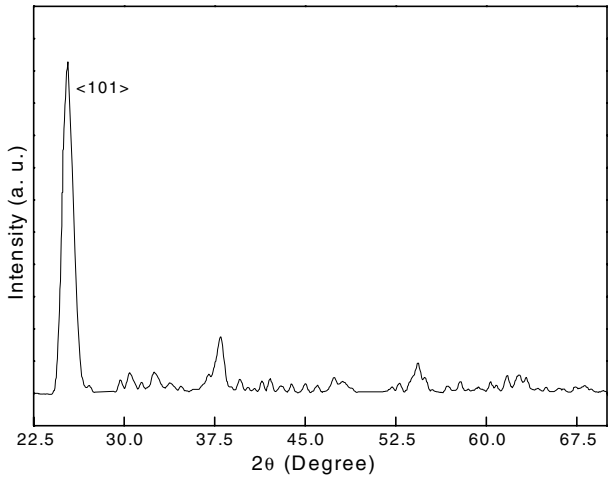

Figure 3. X-ray diffraction pattern of PANI–TiO_2 nanocomposite sample S1.

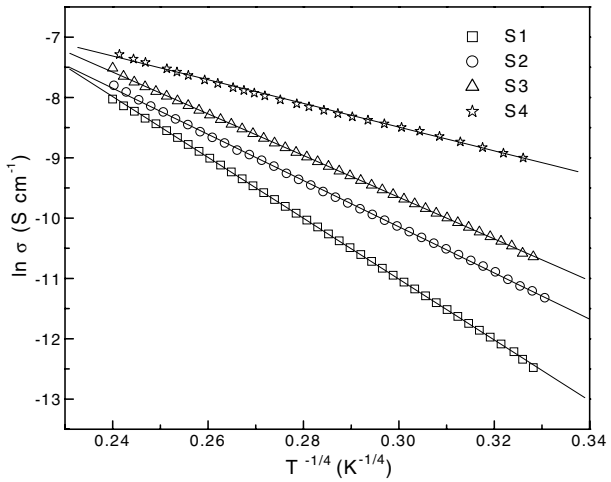

Figure 4. Temperature variation of dc conductivity of samples S1, S2, S3 and S4. The solid lines are fits to equation (2).

PANI are shown in figure 4. The conductivity increases with increases of temperature which is the characteristic behaviour of semiconductors. The temperature dependence of the conductivity $\sigma(T)$ of disordered semiconducting materials is generally described by the Mott variable range hopping (VRH) model [12],

$$\sigma(T) = \sigma_0 \exp[-(T_0/T)^{\gamma}] \qquad (2)$$

where σ_0 is the high temperature limit of conductivity and T_0 is Mott's characteristic temperature associated with the degree of localization of the electronic wavefunction. The exponent $\gamma = 1/(1+d)$ determines the dimensionality of the conducting medium. The possible values of γ are $1/4$, $1/3$ and $1/2$ for three-, two- and one-dimensional systems respectively. The plot of $\ln \sigma(T)$ against $T^{-1/4}$ indicates that three-dimensional (3D) charge transport occurs in all the samples. The values of Mott's characteristic temperature T_0 and the pre-exponential factor σ_0 are obtained from the slopes and intercepts of figure 4 and are given in table 1. The values of T_0 are very sensitive and decrease with increasing PANI content. Both PANI–TiO_2 nanocomposites and pure PANI follow the three-dimensional VRH electrical conduction process.

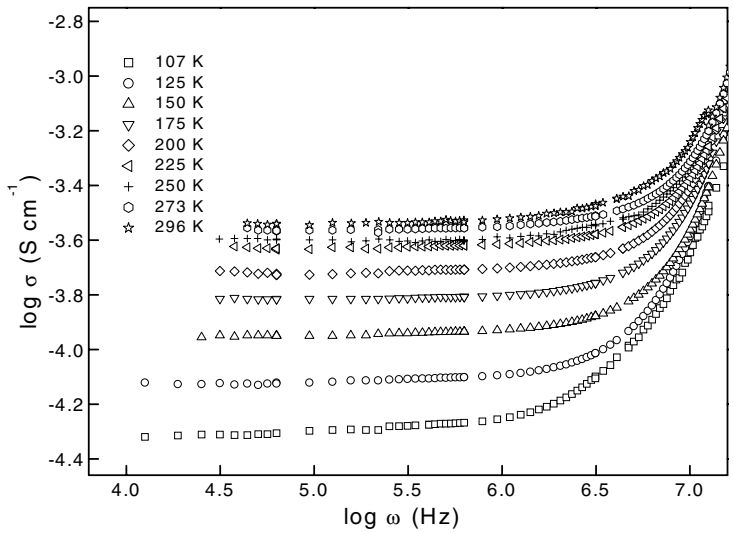

Figure 5. Frequency dependence of conductivity at different temperatures of sample S1.

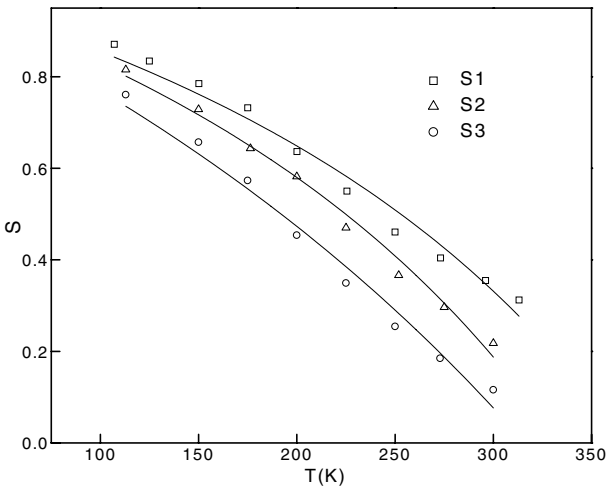

Figure 6. Frequency exponent (S) versus temperature (T) for samples S1, S2 and S3. The solid curves are fits to equation (4).

The ac conductivities of samples S1, S2 and S3 are investigated. The variations of ac conductivity $\sigma(\omega)$ as a function of frequency at different temperatures are shown in figure 5 for sample S1. The plateau observed in $\sigma(\omega)$ at low frequency corresponds to dc conductivity. The conductivity starts to increase from the dc value after a certain characteristic frequency ω_0 known as the cross-over frequency. The plateau region is greater with increasing temperature. The extra contribution to conductivity comes from capacitive regions which provide less impedance at higher frequency. Figure 5 reveals that ω_0 is strongly temperature dependent.

A general feature of amorphous semiconductors and disordered systems is that the frequency dependent conductivity $\sigma(\omega)$ obeys a power law with frequency. The total conductivity $\sigma(\omega)$ at a particular temperature over a wide range of frequencies can be expressed as

$$\sigma(\omega) = \sigma_{\mathrm{dc}} + A\omega^{S} \tag{3}$$

where σ_{dc} is the dc conductivity and A is a constant depending on temperature. The frequency exponent S lies between zero and unity and is given by $S = \mathrm{d}\ln\sigma(\omega)/\mathrm{d}\ln\omega$. The value of S at each temperature has been calculated from the slope of $\log(\sigma_\omega - \sigma_{\mathrm{dc}})$ versus $\log\omega$ plot. The estimated values of S are between 0.1 and 0.9 for all samples as shown in figure 6.

Table 2. Best fitted values of W_{H}, τ_0 of equation (4), hopping length (R_w) and density of states ($N(E_{\mathrm{F}})$) at 107 K.

Sample	W_{H} (eV)	τ_0 (10^{-8} s)	R_w (10^{-2} Å)	$N(E_{\mathrm{F}})$ (10^{27} cm^{-3} eV^{-1})
S1	0.419	71.79	5.43	81.87
S2	0.356	1.648	9.18	16.05
S3	0.253	0.375	22.42	0.838

The microscopic conduction mechanisms of disordered systems are governed by two physical processes such as classical hopping and quantum mechanical tunnelling of charge carries over the potential barrier separating two energetically favourable centres in a random distribution. The exact nature of charge transport is mainly obtained experimentally from the temperature variation of exponent S. The temperature dependences of S for three samples are shown in figure 6. The value of the frequency exponent S decreases with increase of temperature. This behaviour is only observed in the correlated barrier hopping model [13]. The temperature dependence of S based on this model is

$$S = 1 - \frac{6kT}{W_M - kT\ln(\frac{1}{\omega\tau_0})} \tag{4}$$

where W_M is the effective barrier height at infinite intersite separation, τ_0 is the characteristic relaxation time and k is the Boltzman constant. The values of W_M and τ_0 are obtained by the best fitted parameters to equation (4) at a frequency of 100 kHz and are given in table 2. Figure 6 exhibits that the experimental values of S are in good agreement with theoretical model.

The hopping distance (R_ω) at a particular frequency and temperature is [13]

$$R_\omega = \frac{e^2}{\pi\epsilon\epsilon_0}\left[W_M - kT\ln\left(\frac{1}{\omega\tau_0}\right)\right] \tag{5}$$

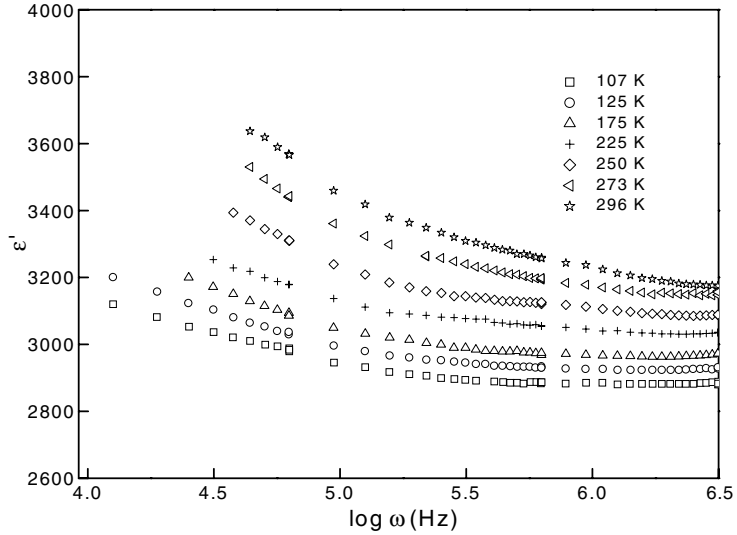

Figure 7. The real part of the dielectric constant versus frequency at different temperatures of sample S1.

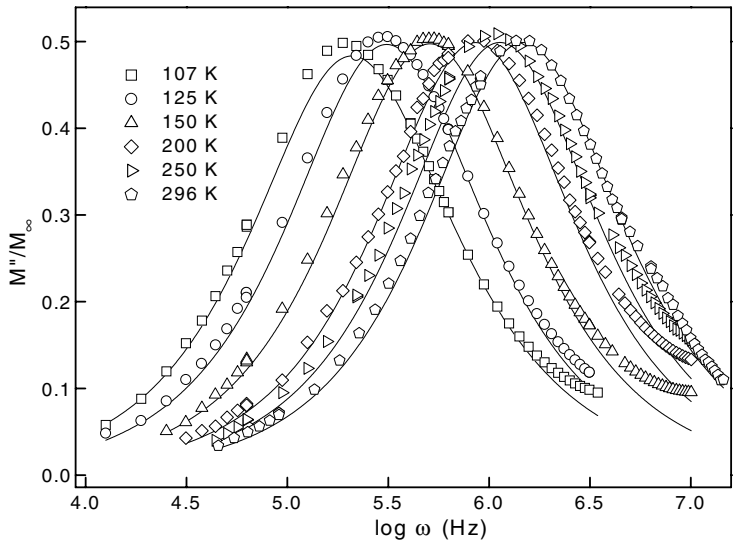

Figure 8. Imaginary part of electric modulus versus frequency plot of sample S1. The solid curves are fits to equation (8).

where e is the electronic charge and ϵ and ϵ_0 are the dielectric permittivity of the material and free space respectively. The calculated hopping distance for different samples are shown in table 2. The value of (R_ω) increases with increasing PANI content.

The expression for ac conductivity in the correlated barrier hopping model is

$$\sigma_1(\omega) = \tfrac{1}{24}\pi^3 N^2 \epsilon\epsilon_0 \omega R_\omega^6 \tag{6}$$

where $N = kTN(E_F)$, and $N(E_F)$ is the density of states at the Fermi level. The best fitted values of W_M and τ_0 are used to calculate $N(E_F)$ from equation (6) and are shown in table 2. With increasing PANI content the density of states decreases, which indicates the existence of delocalized electronic states.

The frequency dependence of the dielectric constant ϵ_1 at several temperatures are presented in figure 7. The interesting fact is that a very high dielectric constant of about 3700 at room temperature is found. The maximum value [14, 15] of the dielectric constant (ϵ_1) in TiO_2 is about 115 and that of PANI [16] is 370. The present observation of ϵ_1 is remarkable as it is larger than the constituent materials. The values of ϵ_1 remain dispersionless over wide range of frequency. The real part of dielectric constant ϵ_1 does not exhibit a sharp decrease with increase of frequency. The values of dielectric constant as a function of aniline content at the lowest measurable frequencies and at room temperature are shown in table 1. The incorporation of TiO_2 nanoparticles increases the magnitude of ϵ_1 significantly compared to pure PANI. The dielectric loss spectra ϵ_2 do not reveal any peak as a function of frequency at all temperatures.

The experimental dielectric data has been analysed using electric modulus formalism M^* which is defined as

$$M^*(\omega) = M' + \mathrm{i}M'' = \frac{1}{\epsilon^*(\omega)} = \frac{\epsilon' + \mathrm{i}\epsilon''}{\epsilon'^2 + \epsilon''^2}. \tag{7}$$

The isothermal imaginary part of M as a function of frequency for sample S1 is depicted in figure 8. The spectra

Table 3. Davidson–Cole (DC) function best fitted parameters τ and β in equation (8) for the dielectric loss spectra of sample S1.

Temperature (K)	τ (10^{-6} s)	β
107	5.06	0.932
125	3.24	0.989
150	1.98	0.999
175	1.46	1
200	1.17	1
225	0.97	1
250	0.88	1
273	0.81	1
296	0.68	1

exhibit broad peaks at low temperature. The peak frequency shifts to higher frequency with increasing temperature.

The relatively large width and asymmetrical nature of the peaks at low temperature suggest a non-Debye behaviour of the dielectric relaxation process. The shape of the M'' peak has been described by the Davidson–Cole (DC) function [17].

$$M^* = M_\infty \left[1 - \frac{1}{(1 + \mathrm{i}\omega\tau)^\beta} \right] \tag{8}$$

where τ is the conductivity relaxation time which is given at the frequency of the maximum of the M'' spectrum. M_∞ is the electric modulus at higher frequency. The parameter β describes the distribution of the relaxation time of the system. Debye relaxation is obtained for $\beta = 1$. The deviation of β from unity indicates the broad distribution of relaxation time in the spectrum. Figure 8 shows that the experimental data are reasonably well fitted with the calculated values of dc function. The best fitted parameters are shown in table 3. The values of β are different from unity, which implies a non-Debye relaxation process at low temperature. Temperature induces the Debye process as confirmed from the values of β at $T \geqslant 175$ K.

The relaxation times, τ, at different temperatures are determined from the reciprocal of the peak frequency. The Arrhenius plot of $\ln \tau$ against $1/T$ for sample S1 is shown in figure 9. A straight line behaviour is obtained. Thus the temperature dependence of the loss relaxation time is given as $\tau \propto \exp(-E/kT)$; E is the activation energy of the dielectric process and k is the Boltzmann constant. The slope of the best fitted straight line gives the activation energy of sample S1, 28.4 meV. The values of activation energy for the other two samples S2 and S3 are 43.9 and 48.8 meV respectively.

The large dielectric constant is found in other materials such as perovskite oxides [18] near the ferroelectric transition and also in high temperature superconductors [19]. The values of ϵ_1 for polymers are very low compared to inorganic materials. Constant efforts are made to increase this value for more technological applications of polymers. The dielectric constant of polymeric systems can generally be enhanced by adding high dielectric constant particulates. Recently it has been observed that the large dielectric constant can be obtained near the percolation threshold of the composite [20]. Commonly, the mechanism for such an enormous value of dielectric constant is Maxwell–Wagner type polarization at the boundary between the metallic electrode and the materials. The temperature dependence of the dielectric constant at low frequency rules out this possibility in the present composites. The nanocomposites consist of two materials having quite

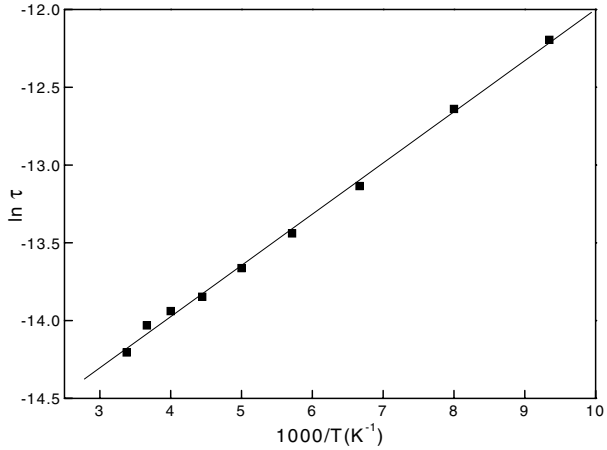

Figure 9. Arrhenius plot of dielectric relaxation time versus frequency at different temperatures for sample S1.

different conductivities and permittivities. The interface across the PANI and TiO_2 may be a source of the large dielectric constant.

5. Conclusion

The dc and ac conductivities have been investigated for different compositions of PANI–TiO_2 nanocomposite. The dc conductivity does not change significantly with PANI concentration. The ac conductivity reveals a correlated barrier hopping type conduction process. The dielectric constant of PANI–TiO_2 is very large and almost independent of frequency. It decreases considerably with increase of PANI content. The presence of TiO_2 nanoparticles does not change the charge transport mechanism of PANI but enhances the dielectric constant by about ten times that of pure PANI. Both the interface and the nanosize of TiO_2 may play important roles to magnify the dielectric properties. The exact physical origins of the huge dielectric constant still remain unclear. However, the large dielectric constant of the nanocomposite provides promising materials for the applications in the fields of micro-actuators, dynamic random access memory and metal oxide semiconductor devices.

Acknowledgments

This work is funded by the Department of Atomic Energy, Government of India (project sanction No 2001/37/4/BRNS). SD is grateful to the Council of Scientific and Industrial Research, Government of India, for providing a fellowship.

References

[1] Skothemin T and Elsenbaumer R 1998 *Handbook of Conducting Polymers* (New York: Dekker)
[2] Hua Z, Shi J, Zhang L, Ruan M and Yan J 2002 *Adv. Mater.* **14** 830
[3] Rothschold A and Komem Y 2003 *Appl. Phys. Lett.* **82** 574
[4] Gangopadhyay R and De A 2003 *H-Conducting Polymer Nanocomposites (Handbook of Organic–Inorganic Hybrid Materials and Nanocomposites)* ed H S Nalwa (CA: American Scientific Publishers)
[5] Somani P R, Marimuthu R, Mulik U P, Sainkar S R and Amalnekar D P 1999 *Synth. Met.* **106** 45

[6] Su S and Kuramoto N 2000 *Synth. Met.* **114** 147
[7] Xia H and Wang Q 2002 *Chem. Mater.* **14** 2158
[8] Li X, Chen W, Bian C, He J, Xu N and Xue G 2003 *Appl. Surf. Sci.* **217** 16
[9] Zhang J, Ju X, Wang B, Li Q, Liu T and Hu T 2001 *Synth. Met.* **118** 181
[10] Elim H, Ji W, Yuyono A H, Xue J M and Wang J 2003 *Appl. Phys. Lett.* **82** 2691
[11] Klug H P and Alexander L E 1954 *X-ray Diffraction Procedures for Polycrystalline and Amorphous Materials* (New York: Wiley) p 491
[12] Mott N F and Davis E 1979 *Electronic Process in Non Crystalline Materials* 2nd edn (Oxford: Clarendon)
[13] Elliott S R 1987 *Adv. Phys.* **37** 135
[14] Paily R, Dasgupta A, Dasgupta N, Bhattacharya P, Misra P, Ganguli T, Kukreja L M, Balamurugan A K, Rajagopalan S and Tyagi A 2002 *Appl. Surf. Sci.* **187** 297
[15] Van Dover R V 1999 *Appl. Phys. Lett.* **74** 3041
[16] Zuo F, Angelopoulos M, MacDiarmid A G and Epstein A J 1989 *Phys. Rev.* B **39** 3570
[17] Davidson D W and Cole R H 1950 *J. Chem. Phys.* **18** 1417
[18] Lunkenheimer P, Bobnar V, Prinin A V, Ritus A I, Volkov A A and Loidl A 2002 *Phys. Rev.* B **66** 052105
[19] Cao G, O'Reilly J, Crow J and Testardi L 1993 *Phys. Rev.* B **47** 11510
[20] Huang C, Zhang Q and Su J 2003 *Appl. Phys. Lett.* **82** 3502